Quadrupolar superexchange interactions, multipolar order, and magnetic phase transition in UO_2

Leonid V. Pourovskii[1,2] and Sergii Khmelevskyi[3]
[1]*CPHT, Ecole Polytechnique, CNRS, Université Paris-Saclay, Route de Saclay, 91128 Palaiseau, France*
[2]*Collège de France, 11 place Marcelin Berthelot, 75005 Paris, France*
[3]*Center for Computational Materials Science, IAP, Vienna University of Technology, Vienna, Austria*

(Received 5 October 2018; revised manuscript received 15 February 2019; published 29 March 2019)

The origin of noncollinear magnetic order in UO_2 is studied by an *ab initio* dynamical-mean-field-theory framework in conjunction with a linear-response approach for evaluating intersite superexchange interactions between U $5f^2$ shells. The calculated quadrupole-quadruple superexchange interactions are found to unambiguously resolve the frustration of face-centered-cubic U sublattice toward stabilization of the experimentally observed noncollinear 3**k**-magnetic order. Therefore, the exotic 3**k**-antiferromagnetic order in UO_2 can be accounted for by a purely electronic exchange mechanism acting in the undistorted cubic lattice structure. The quadrupolar short-range order above magnetic ordering temperature T_N is found to qualitatively differ from the long-range order below T_N.

DOI: 10.1103/PhysRevB.99.094439

I. INTRODUCTION

The interplay of local spin and orbital degrees of freedom (DOF) in strongly correlated electron systems is at the origin of such remarkable phenomena as the multiferroic behavior [1], dynamical single-ion and cooperative Jahn-Teller effects [2], and colossal magnetoresistance [3]. In rare-earth and actinides compounds with localized f shells a strong spin-orbit coupling (SOC) in conjunction with the crystal-field (CF) splitting may lead to emergence of local multipolar DOF. Intersite interactions between such multipolar moments in many cases result in their ordering; exotic multipolar-ordered (MO) states might coexist with the usual magnetic one [4]. The rich physics of the multipolar DOF in f-electron systems ranges from the quadrupole interaction mediated superconductivity [5] and quadrupolar Kondo effects [6] to phonon-mediated electric multipolar interactions and the dynamical Jan-Teller effect. Multipolar order parameters are invisible to conventional neutron-diffraction probes and thus notoriously difficult to unambiguously identify experimentally. The quantitative modeling of MO phenomena also represents a significant theoretical challenge due to a large number of multipolar DOF and a rather small magnitude of relevant energy scales compared to the conventional Heisenberg dipole-dipole couplings [7].

The uranium dioxide is a prototypical example of the MO in actinide magnetic insulators [4,7]. It has a simple cubic fluorite structure, where U atoms occupy the fcc sublattice (see Fig. 1). Due to its importance as a nuclear fuel [8] and chemical catalyst [9] it has been thoroughly studied experimentally. UO_2 undergoes a first-order phase transition into an antiferromagnetically (AFM) ordered state at the Néel temperature T_N of 30.8 K [10]. This transition is accompanied by an onset of MO [11] affecting both phonons and magnons dynamics [4,7,12,13]. Dynamical Jahn-Teller effects associated with a spin-lattice quadrupolar coupling is also observed well above T_N [10,12].

The magnetic structure of UO_2 has been an experimental and theoretical puzzle for a long time. The magnetic unit cell of UO_2 in the AFM phase contains four inequivalent simple cubic uranium sublattices. Then the geometrical frustration of the U fcc sublattice results in three distinct AFM structures shown in Fig. 1 being degenerate in energy with respect to the usual spin-spin anisotropic Heisenberg exchange [14]. These structures are described, respectively, by (a) the single propagation vector $\mathbf{k} = [0, 0, 1]$ (1**k**-collinear structure in the upper panel of Fig. 1), (b) two propagation **k** vectors (2**k**, middle panel of Fig. 1) with mutually perpendicular orientations of the magnetic moments in the cubic face plane parallel to the plane of the **k** vectors, and (c) three perpendicular **k** vectors (3**k**, lower panel) with the moments oriented in different (111) directions [14]. All three AFM structures have been observed in different cubic uranium monopnictides (UX with X = N, P, As, Sb) [14]. The 3**k** structure has been finally confirmed to be the magnetic ground state of UO_2 by neutron diffraction and nuclear magnetic resonance experiments [10,15,16].

The mechanism leading to the stabilization of noncollinear 3**k** AFM in UO_2 has not been clearly identified to date. The crystal field splitting obtained in various experiments suggests that the ground state of the U^{4+} ions in UO_2 is a spherically symmetric Γ_5 triplet well separated from excited CF states [10,17], thus the observed AFM structure cannot be due to the single-ion anisotropy. The lattice induced quadrupole-quadrupole (QQ) coupling might explain the first-order nature of the magnetic transition in UO_2, however, it seems to favor the 1**k** structure rather than the 3**k** one [18,19]. Hence, the 3**k** AFM should be rather due to a purely electronic mechanism with lattice distortions subsequently induced by the magnetic ordering [18]. The electronic quadrupolar superexchange (SE) can in principle stabilize the 3**k**-magnetic order in the structurally undistorted high-temperature phase as suggested by Ref. [20]. They supported this conjuncture with a rather crude estimation of SE interactions (SEI) within a semiempirical kinetic exchange model.

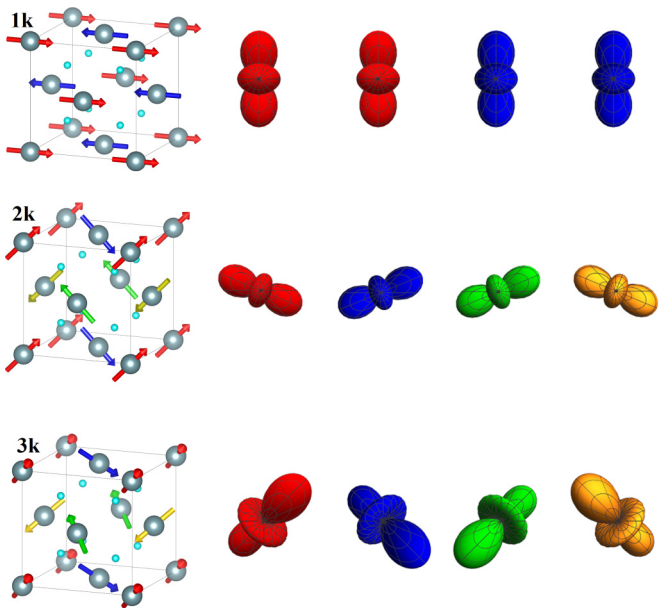

FIG. 1. 1**k** (upper panel), 2**k** (middle panel), and 3**k** (lower panel) antiferromagnetic orders in the unit cell of UO_2. Uranium and oxygen sites are shown as large gray and small cyan balls, respectively. The quadrupole moments on inequivalent simple-cubic sublattices of the magnetic cell obtained by the mean-field solution of the *ab initio* SE Hamiltonian, Eqs. (3) and (4), at $T = 0$ for each antiferromagnetic structure are displayed on the right-hand side and colored to indicate the corresponding U site in the unit cell.

A reliable estimation of the QQ superexchange couplings in UO_2 is thus crucial to unravel the origin of its unusual noncollinear order. The theoretical evaluation of MIs by *ab initio* density-functional-theory (DFT) methods have a recognized vital importance in the field (see Refs. [21,22] for review). However, the standard DFT framework in conjunction with local or semilocal exchange correlation functionals is not applicable to localized U $5f$ states in UO_2. The DFT+U method, which was extensively employed to study UO_2 [23–25], is able to capture this localization, but only in the symmetry-broken ordered state. Pi *et al.* [26] has recently developed an approach for evaluating MIs based on a simultaneous flip of multipolar moments on two sites in a MO state described within DFT+U. Pi *et al.* [26,27] predicted the spin-wave spectra of UO_2 in reasonable agreement with experiment, but their calculated SE QQ interactions are ferromagnetic and would favor the 1**k** AFM magnetic order instead of the 3**k** one.

Both the high-temperature paramagnetic phase and ordered states of correlated f compounds can be in principle quantitatively described by combining DFT with the dynamical mean-field theory (DMFT) [28] treatment of localized f shells. This DFT+DMFT method [29–31] has been extensively employed to study the electronic structure of paramagnetic UO_2 [32,33]. However, low symmetries, small energy scales, and a vast configurational space of MO phases render a direct application of DFT+DMFT to the symmetry-broken phase of UO_2 difficult.

In this work we first derive the *ab initio* electronic structure and CF splitting of UO_2 in its paramagnetic cubic phase and then apply the linear-response post-processing of Ref. [34] to these converged DFT+DMFT results evaluating all relevant dipole and multipole SEIs for the CF ground state. The resulting *ab initio* SE Hamiltonian is then solved within the mean-field approximation. We find that its most stable ordered structure is of the noncollinear 3**k** type and that its stabilization originates from a particular anisotropy of quadrupole-quadrupole SEIs in UO_2.

The paper is organized as follows: in the next section we outline the methodology of our electronic structure and superexchange calculations also specifying relevant calculational parameters. The results of these calculations, namely the *ab initio* superexchange Hamiltonian of UO_2 and its mean-field solution, are presented in Sec. III. In Sec. IV we analyze the calculated superexchange interactions identifying a mechanism for the stabilization of 3**k** magnetic order and also study short-range order effects in UO_2 above its ordering temperature.

II. METHOD

Our self-consistent in the charge density DFT+DMFT calculations were carried out employing the approach of Refs. [35,36], which combines a linearized augmented plane-wave band structure method [37] and the DMFT implementation [38,39]. The spin-orbit coupling for the UO_2 Kohn-Sham band structure was included within the standard second-variation procedure as implemented in Ref. [37], which is expected to be sufficient for the valence (but not semicore) states of uranium.

Wannier orbitals $\omega_{m\sigma}$ representing U $5f$ states (where m and σ are magnetic and spin quantum numbers, respectively) were constructed from the manifold of 14 Kohn-Sham $5f$-like bands located in the vicinity of the Fermi level. The on-site repulsion between these orbitals was specified by the Slater parameters F^0, F^2, F^4, and F^6. We made use of the standard approximation fixing the ratios of F^2/F^4 and F^2/F^4 to the values obtained in Hartree-Fock calculations for the corresponding free ions. We employ the ratios of 1.50 and 2.02, respectively, in good agreement with the values for actinide ions reported, for example, in Ref. [40]. With this choice the values of F^2, F^4, and F^6 are determined by the Hund's rule coupling J_H [29]. We used $F^0 = 4.5$ eV and $J_H = 0.6$ eV obtained for UO_2 in recent constrained random-phase calculations [41]. SEIs can exhibit a strong sensitivity to the value of J_H, hence, to verify the robustness of our results we also performed calculations with $J_H = 0.7$ eV previously employed in Ref. [26].

The DMFT quantum impurity problem was solved in the quasiatomic Hubbard-I approximation (HIA) [42], which is expected to be reasonable for the paramagnetic high-T phase of the Mott insulator UO_2. The hybridization function is neglected within the HIA, and the DMFT impurity problem is reduced to diagonalization of the single-shell Hamiltonian $\hat{H}_{\rm at} = \hat{H}_{\rm 1el} + \hat{H}_{\rm U} = \sum_{mm'\sigma\sigma'} \epsilon^{\sigma\sigma'}_{mm'} f^{\dagger}_{m\sigma} f_{m'\sigma'} + \hat{H}_{\rm U}$, where $f_{m\sigma}$ ($f^{\dagger}_{m\sigma}$) is the creation (annihilation) operator for the U $5f$ orbital $m\sigma$, $\hat{H}_{\rm U}$ is the on-site Coulomb repulsion vertex constructed as described above, and $\hat{\epsilon}$ is the noninteracting level position matrix [30]. In the DMFT framework $\hat{\epsilon}$ obtained by a high-frequency expansion of the bath Green's function

[43] reads

$$\hat{\epsilon} = -\mu + \langle \hat{H}_{\rm KS} \rangle^{ff} - \Sigma_{\rm DC}, \quad (1)$$

where μ is the chemical potential, $\langle \hat{H}_{\rm KS} \rangle^{ff} = \sum_{\mathbf{k}\in \rm BZ} \hat{P}_{\mathbf{k}} H^{\mathbf{k}}_{\rm KS} \hat{P}^{\dagger}_{\mathbf{k}}$ is the Kohn-Sham Hamiltonian projected to the basis of $5f$ Wannier orbitals $\omega_{m\sigma}$ and summed over the Brillouin zone, $\hat{P}_{\mathbf{k}}$ is the corresponding projector between the KS and Wannier spaces [35,39], and $\Sigma_{\rm DC}$ is the double-counting correction term. As the spin-orbit coupling is included in the Kohn-Sham states it naturally appears in $\hat{\epsilon}$ together with the crystal-field splitting. The double-counting correction $\Sigma_{\rm DC}$ was calculated in the fully localized limit [44] using the atomic occupancy [43] of the U $5f^2$ shell.

The DFT+DMFT self-consistent calculations employing the HIA (we abbreviate this framework DFT+HIA below) were carried out enforcing the uniform occupancy of U $5f^2$ states within its ground-state multiplet (GSM) in order to suppress the impact of DFT self-interaction error onto the CF splitting [45] and at the experimental lattice parameter $a = 5.47$ Å of UO_2.

In order to evaluate dipole and quadrupole SEIs acting between U shells in UO_2 state we employed the method of Ref. [34]. Namely, after having converged DFT+HIA for the symmetry-unbroken paramagnetic state one evaluates the linear response of the DFT+DMFT grand potential Ω to small fluctuations of the on-site density matrix on two neighboring sites $\mathbf{R}$ and $\mathbf{R}'$ with respect to its paramagnetic configuration. These fluctuations are assumed to be limited to the ground-state (GS) crystal-field (CF) level for the cases when the magnitude of SEIs is much smaller than that of the CF splitting.

The corresponding variational derivative of the DFT+DMFT grand potential with respect to such fluctuations $\frac{\delta^2\Omega}{\delta\rho^{\alpha\beta}(\mathbf{R})\delta\rho^{\gamma\delta}(\mathbf{R}')}$ is then identified as the matrix element $\langle\alpha\gamma|V(\mathbf{R}'-\mathbf{R})|\beta\delta\rangle$ of SEI $V(\mathbf{R}'-\mathbf{R})$ between the two-site states $|\alpha\gamma\rangle$ and $|\beta\delta\rangle$. The first and second letter in $|\cdots\rangle$ labels a given CF state of the CF GS level on the ions $\mathbf{R}$ and $\mathbf{R}'$, respectively. The lowercase Greek letters designate states within the GS CF level, and $\hat{\rho}$ is the density matrix for the GS CF level. The dependence of V on $\mathbf{R}'-\mathbf{R}$ only is due to the translational invariance. As shown in Ref. [34], $\frac{\delta^2\Omega}{\delta\rho^{\alpha\beta}(\mathbf{R})\delta\rho^{\gamma\delta}(\mathbf{R}')} = \frac{1}{\beta}\mathrm{Tr}[G_{\mathbf{R}\mathbf{R}'}\frac{\delta\Sigma}{\delta\rho^{\gamma\delta}}G_{\mathbf{R}'\mathbf{R}}\frac{\delta\Sigma}{\delta\rho^{\alpha\beta}}]$, where the variational derivative of the local self-energy Σ with respect to a given fluctuation $\rho^{\alpha\beta}$ of the density matrix is evaluated analytically within the HIA. The intersite Green's function (GF) $G_{\mathbf{R}\mathbf{R}'}$ is obtained by a Fourier transform of the lattice GF projected to the basis of correlated $5f$ orbitals.

III. RESULTS

We start by discussing the electronic structure and many-electron states of U $5f$ shell as obtained by the DFT+HIA method for the paramagnetic phase of UO_2. In Fig. 2 we display the calculated valence-band spectral function compared to recent photoemission (PES) and bremsstrahlung isochromat spectra (BIS) of Ref. [46]. These experimental measurements employed high photon energies thus enhancing the relative spectral weight of $5f$ features. Our calculated valence-band spectral function is in an overall qualitative agreement with the experimental results of Ref. [46]. The width of the U $5f$ upper Hubbard band is mostly due to multiplet effects and in agreement with the experimental spectra, while the width of the lower Hubbard band is due to hybridization effects and underestimated due to well-known limitations of the Hubbard-I approximation [47]. The overall splitting between upper and lower Hubbard bands and the multiplet splitting of excited states that are crucial to correctly capture the superexchange phenomenon are quantitatively well reproduced by our approach.

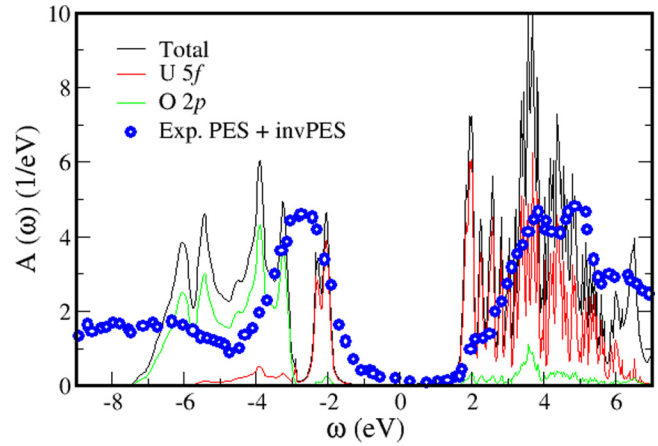

FIG. 2. The DFT+DMFT spectral function of UO_2 within the Hubbard-I approximation. The black, red, and green lines are the total, partial U $5f$, and O $2p$ spectral functions, respectively. The experimental emission and bremsstrahlung isochromat spectra of Ref. [46] are displayed by blue circles.

As outlined in the Method section, the DMFT impurity problem within the HIA is reduced to a single $5f$ shell Hamiltonian $\hat{H}_{\rm at}$, its one-electron level positions (1) includes both the spin-orbit and crystal-field effects. The value of spin-orbit coupling parameter $\lambda = 0.235$ eV extracted from our converged $\hat{\epsilon}$ is in agreement with Hartree-Fock calculations for free U ion [48]. It is expected that λ being an essentially intra-atomic quantity is not significantly affected by the solid-state environment. By diagonalizing $\hat{H}_{at}$ we obtained the $^3H_4$ ground-state multiplet (GSM) of U $5f^2$ shell with the Γ_5 triplet being the CF ground state; the exited doublet Γ_3, triplet Γ_4, and singlet Γ_1 predicted to be 193, 197, and 207 meV higher in energy, respectively. Our theoretical CF splitting is thus in good agreement with experimental measurements [17] that found the splitting of 150 to 180 meV between the Γ_5 ground state and densely spaced exited CF levels, as well as with previous DMFT calculations of Ref. [32]. This CF splitting is much higher than T_N of UO_2, hence, the impact of exited multiplets on the magnetic order can be neglected.

The calculated Γ_5 eigenstates in the $|J;m_J\rangle$ basis

$$\begin{aligned} |1\rangle &= 0.908|4;+3\rangle - 0.343|4;-1\rangle - 0.032|5;-5\rangle, \\ |0\rangle &= 0.686|4;+2\rangle - 0.686|4;-2\rangle - 0.033|5;-2\rangle \\ &\quad - 0.033|5;+2\rangle, \\ |-1\rangle &= -0.908|4;-3\rangle + 0.343|4;+1\rangle - 0.032|5;+5\rangle \end{aligned} \quad (2)$$

feature a small admixture of high-energy multiplets.

TABLE I. Calculated U-U nearest-neighbor interactions for the [1/2,1/2,0] bond (meV) as a function of the Hund's rule coupling J_H.

J_H (eV)	V	V'	$V_{x,y}$	V^q_{xy}	$V^q_{xz(yz)}$	$V^q_{x^2-y^2}$	$V^q_{z^2}$	$V^q_{xz,yz}$
0.6	1.42	3.85	−0.67	0.18	0.01	−0.16	0.14	0.04
0.7	1.39	3.73	−0.69	0.20	0.01	−0.18	0.17	0.04

We calculated the SEIs between the Γ_5 states (2) by the approach of Ref. [34] outlined in the Method section. There are in total $3^4 = 81$ SEIs $\langle\alpha\gamma|V(\mathbf{R}'-\mathbf{R})|\beta\delta\rangle$ for each U-U bond. We have subsequently transformed these interactions to more conventional SE couplings between the spherical tensor dipole and quarupole moments. The Γ_5 triplet (effective angular momentum $\tilde{J}=1$) can support both dipole and quadrupole moments [49]. The SEIs between those moments were obtained using the transformation $\sum_{\alpha\beta\gamma\delta}\langle\beta\delta|V(\mathbf{R}'-\mathbf{R})|\alpha\gamma\rangle O^{LM}_{\alpha\beta}O^{L'M'}_{\gamma\delta} = V^{LL'}_{MM'}(\mathbf{R}'-\mathbf{R})$, where $O^{LM}_{\alpha\beta}$ is the $\alpha\beta$ matrix element of the real spherical tensor for the effective angular momentum $\tilde{J}=1$ [4,34] of the rank $L=1$ (dipole) or 2 (quadrupole) and projection M. $V^{LL'}_{MM'}(\mathbf{R}'-\mathbf{R})$ is the resulting SEI between the multipoles LM and $L'M'$ located at the sites $\mathbf{R}$ and $\mathbf{R}'$, respectively.

Thus calculated SE Hamiltonian for the nearest-neighbor (NN) U-U bond $\mathbf{R}'-\mathbf{R}=[1/2,1/2,0]$ is of the form $H_{\rm SE} = H_{\rm DD}+H_{\rm QQ}$, where the dipole-dipole (DD) and QQ contributions (in the global coordinate system) read

$$H_{\rm DD} = V\sum_{M=x,y}\hat{O}^M_{\mathbf{R}}\hat{O}^M_{\mathbf{R}'} + V'\hat{O}^z_{\mathbf{R}}\hat{O}^z_{\mathbf{R}'} + V_{x,y}\left[\hat{O}^x_{\mathbf{R}}\hat{O}^y_{\mathbf{R}'}+\hat{O}^y_{\mathbf{R}}\hat{O}^x_{\mathbf{R}'}\right], \quad (3)$$

$$H_{\rm QQ} = \sum_{M\in t_{2g},e_g} V^q_M\hat{O}^M_{\mathbf{R}}\hat{O}^M_{\mathbf{R}'} + V^q_{xz,yz}\left[\hat{O}^{xz}_{\mathbf{R}}\hat{O}^{yz}_{\mathbf{R}'}+\hat{O}^{yz}_{\mathbf{R}}\hat{O}^{xz}_{\mathbf{R}'}\right]. \quad (4)$$

The number of independent SE couplings is seen to be significantly reduced due to the cubic symmetry of the problem. Hence, for brevity we omit the rank L in the real tensors, as the projection M is sufficient to identify them unambiguously, and suppress superfluous indices for V. The QQ SEI are labeled by the superscript q. SE Hamilonians for other NN bonds are easily obtained from (3) and (4) by symmetry. Our choice for the spherical tensors representing the dipole and quadrupole DOFs of the Γ_5 triplet is in agreement with Refs. [26,27], however, following Santini *et al.* [4] we employ $\hat{O}$ to denote real spherical tensors instead of $\hat{T}$ in Refs. [26,27]. The operator notation is also employed in the literature [7,20,50] for the low-energy Hamiltonian of UO_2. SEIs in the operator formalism are related to the tensor SEIs in (4) by a simple renormalization that we specify in Appendix A. The interactions of next-nearest neighbors (NNN) are an order of magnitude smaller and induce no qualitative changes, they are listed in Appendix B. More distant SEIs are negligible. The calculated NN SEIs for two values of J_H are listed in Table I. One may see that the variation in J_H has a rather insignificant impact on the SEIs. Unless explicitly mentioned otherwise, we use the SEIs for $J_H = 0.6$ eV in all calculations below.

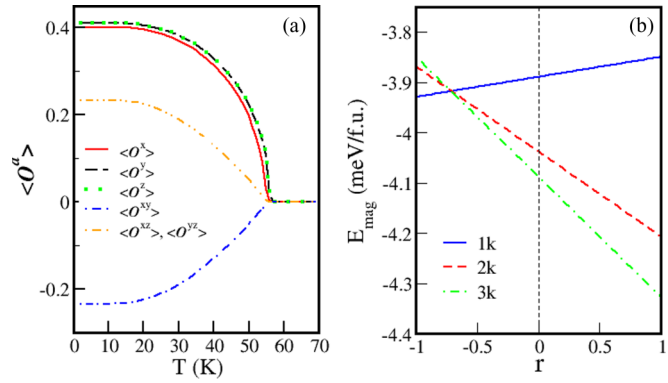

FIG. 3. (a) The expectation values of dipole and t_{2g} quadrupole tensors as a function of temperature. A phase transition at $T = 56$ K is clearly seen. (b) The mean-field magnetic energy $E_{\rm mag}$ at zero temperature as a function of the anisotropy parameter r of the QQ SE, see text.

We have subsequently solved the calculated *ab initio* SE Hamiltonian including NN and NNN couplings within the mean-field approximation (MFA) implemented in Ref. [51]. We considered three structures shown in Fig. 1 as well as all single-**k** magnetic structures realizable within the $4\times4\times4$ fcc supercell. A clear phase transition is observed in the evolution of specific heat at about $T_N = 56$ K (with only NN SEIs $T_N = 60$ K) accompanied by appearance of a nonzero on-site dipole moment oriented along the $\langle111\rangle$ direction and quadrupole moments of the t_{2g} irreducible representation (IREP) as shown in Fig. 3(a) [52]. The obtained magnetic and quadrupole orders correspond to the 3**k** structure plotted the lower panel of Fig. 1, which is the experimental ordered structure of UO_2. Predicted T_N is substantially higher than the experimental first-order transition temperature of 30.8 K. A large overestimation of T_N in the MFA is expected for the fcc lattice due to its geometric frustration [53,54].

IV. ANALYSIS AND DISCUSSION

Let us now analyze the calculated SEIs in order to identify the origin of 3**k**-structure stabilization with respect to the competing 1**k** and 2**k** ones. The DD interactions are antiferromagnetic and very asymmetric. With $J' < J < 0$ all three AFM structures shown in Fig. 1 become degenerated with respect to $H_{\rm DD}$ (3) having the same ordering energy $E_{\rm mag} = -V' = -3.85$ meV/f.u. in the mean-field approximation [18,55]. The quadrupole orders shown on the right-hand side of Fig. 1 are obtained by solving the full SE NN Hamiltonian for the AFM state of a given type. With the calculated SE QQ interactions from Table I the QQ contribution to the ground state energies is equal to 0.010, −0.047, and −0.060 meV/(f.u.) for the 1**k**, 2**k**, and 3**k** orders, respectively.

Therefore we conclude that the QQ SEI are stabilizing the experimentally observed noncollinear 3**k** magnetic structure in the absence of an SL mediated contribution; this order of a purely electronic origin would subsequently result in the Jahn-Teller distortion. The SL QQ coupling, however, might be essential for the full description of the relative stability of

TABLE II. Comparison of the SEI calculated in the present work with previous DFT+U calculations of Ref. [27], and the values of Ref. [7] from a fit of the experimental spin-wave spectra. Following Refs. [7,27] we define the isotropic part of DD and QQ SEIs as V' and V^q_{xy}, respectively. and the corresponding dimensionless anisotropy parameters $\delta^{d/q}$ defined as $\delta^d = V/V'$ and $\delta^q = V^q_{yz}/V^q_{xy}$, respectively. References [7,27] estimated only the SEI is relevant for the 3**k** structure, thus only those four parameters are available for comparison (note that Ref. [7] assumed $\delta^q = \delta^d$).

	V'	δ^d	V^q_{xy}	δ^q,
This work	3.85	0.37	0.18	0.22
Ref. [7]	3.1	0.25	1.9	0.25
Ref. [27]	1.70	0.3	−3.10	0.9

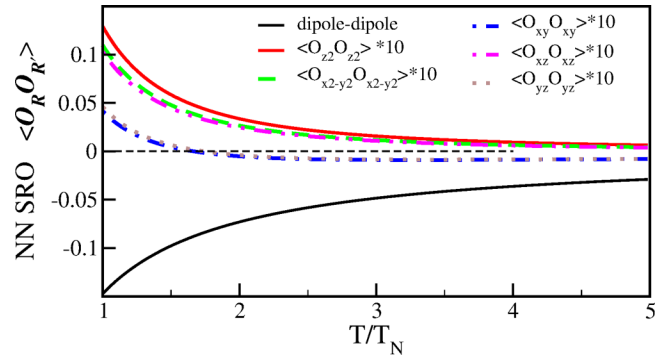

FIG. 4. The dipole-dipole and quadrupole-quadrupole nearest-neighbor pair correlation functions above T_N. The quadrupole-quadrupole pair correlation functions are multiplied by 10.

ordered magnetic structures as well as for the spin dynamics in UO_2 [7,50].

In Table II we compare our results to previous theoretical and experimental estimates of SEIs in UO_2. Our DD SE is very close to the fit of experimental spin-waves spectra of Ref. [7], however, our QQ SEIs are much smaller. The qualitative difference with the DFT+U results [27] is in the sign of the QQ interactions. The negative sign predicted in Ref. [27] would stabilize 1**k** order having NN $\langle \hat{O}^M_{\mathbf{R}} \hat{O}^M_{\mathbf{R}'} \rangle = 0$ for all M belonging to the t_{2g} IREP (xy, xz, yz). AF t_{2g} SEIs favor the 3**k** structure because of a larger angle between ordered quadrupoles in this case as compared to the 2**k** structure, where one third of NN pairs have parallel quadrupole moments and the 1**k** structure, where all quadrupole moments are parallel (see Fig. 1).

The magnitude of SEIs acting between the e_g quadrupoles has not been evaluated in Ref. [27] neither can it be estimated from the spin-wave dispersion, as $\langle \hat{O}^M_{\mathbf{R}} \hat{O}^M_{\mathbf{R}'} \rangle = 0$ for $M = z^2$ and $x^2 - y^2$ in the experimental 3**k** AFM structure. However, the contribution of e_g SEIs is nonzero for the 1**k** and 2**k** competing orders thus impacting the relative stability of magnetic structures.

In order to further clarify the impact of QQ SEIs on the relative stability of these three structures one may evaluate their single-site mean-field Hamiltonian in a local coordinate frame [50], in which the on-site dipole moment is parallel to the local z axis. In such a frame only the z^2 quadrupole is active, while other local quadrupole moments are zero thus simplifying the analysis (see Appendix A for the definition of quadrupole moments in terms of spin operators). The mean-field Hamiltonian reads $\hat{H}_{\rm MF} = \hat{H}^{\rm MF}_{\rm DD} + \hat{H}^{\rm MF}_{\rm QQ}$, where the dipole-dipole contribution $\hat{H}_{\rm DD} = -4V' \langle \hat{O}^z_l \rangle \hat{O}^z_l$ is the same for all three structures. $\hat{O}^z_l$ is the z projection of the dipole tensor operator in the local frame, its expectation value $\langle \hat{O}^z_l \rangle = 1/\sqrt{2}$ at the full saturation.

The QQ term $\hat{H}^{\rm MF}_{\rm QQ}$ reads $V_{QQ} \langle \hat{O}^{z^2}_l \rangle \hat{O}^{z^2}_l$, where the quadrupole operator $\hat{O}^{z^2}_l$ is defined in the local frame in the same way as the dipole one. The mean-field QQ coupling $V_{\rm QQ}$ is equal to $6V^q_{e_g}$, $(\frac{3}{8\sqrt{2}} + \frac{9}{8})V^q_{e_g} - 3V^q_{xy}$, and $-4V^q_{xy}$ for the 1**k**, 2**k**, and 3**k** orders, respectively. Here we designate as $V^q_{e_g} = V^q_{z^2} + V^q_{x^2-y^2}$ the summed diagonal SEI between e_g quadrupoles. One sees that the relative stability of the structures is determined by the relative magnitudes of $V^q_{e_g}$ and the in-plain coupling between t_{2g} quadrupoles V^q_{xy}. In particular, the opposite signs of our calculated $V^q_{z^2}$ and $V^q_{x^2-y^2}$ result in the magnitude of $V^q_{e_g} = -0.02$ meV that is much smaller than $V^q_{xy} = 0.18$ meV. While $V^q_{e_g}$ is negative and does help stabilizing 1**k** and 2**k** structures, its contribution is overweighted by a larger prefactor for V^q_{xy} in the case of 3**k**. Therefore, it is the particular anisotropy of QQ SEIs of UO_2 with a larger magnitude of positive $V^q_{t_{2g}}$ that is at the origin of 3**k** order in UO_2.

From the mean-field Hamiltonian derived above one may easily evaluate the effect of a variation in the relative value of the QQ SEIs $V^q_{e_g}$ and V^q_{xy} on the ground-state magnetic structure of UO_2. One may introduce renormalized SEIs $V^q_{e_g}(1-r)$ and $V^q_{xy}(1+r)$ with $r \in [-1:1]$. Hence, $r = 0$ corresponds to the actual calculated QQ SEIs, while at $r = -1$ (1) only $V^q_{e_g}$ (V^q_{xy}) are nonzero. The resulting evolution of the mean-field ordering energy $E_{\rm mag}$ vs r is plotted in Fig. 3(b). One finds that the 1**k** is stabilized with $r \to -1$, while the actual 3**k** is stabilized in the opposite limit. At $r \approx -0.713$ one obtains a transition between the 1**k** and 3**k** orders. Interestingly, the 2**k** structure is unstable relative to the 1**k** order for $r < -0.707$ and relative to the 3**k** one for $r > -0.732$, meaning that over the whole range of r the ground state is never of the 2**k** type.

The phase transition in UO_2 is of the first order and dynamical Jahn-Teller effects are also observed well above T_N [10,12] hinting at a non-negligible short-range order (SRO) present in UO_2. We have analyzed SRO effects above the Néel temperature using an Oguchi-like method [56]. To this end we diagonalized the *ab initio* SE Hamiltonian, Eqs. (3) and (4), with the SEIs from Table I, for each NN pair of U ions. We then calculated the DD and QQ pair correlation functions $\langle \hat{O}^M_{\mathbf{R}} \hat{O}^{M'}_{\mathbf{R}'} \rangle$ by averaging them over all NN bonds. The calculated NN pair correlation functions vs T/T_N are shown in Fig. 4. Strong dipole SRO effects are clearly observed well above Néel temperature as expected for the frustrated fcc lattice [57]. The dominating AFM dipole SRO forces a ferro-quadrupole SRO for both the t_{2g} and e_g quadrupoles for $T > T_N$ as one sees in Fig. 4. The constrain of antiparallel orientation of the neighboring dipole moments is lifted in the ordered state by the AFM frustration. The t_{2g} quadrupole order is then antiferro due to the corresponding sign of QQ SEIs, while the e_g pair correlation functions are zero. Hence, the structure of

QQ pair correlation function below and above the phase transition is qualitatively different. This observation has two important consequences. First, a SRO that is opposite to the corresponding pair correlation function in the ordered state is associated with a first-order magnetic phase transition [58–60]. This hints at a purely electronic SE mechanism for the observed first-order type of magnetic transition in UO_2. Second, the dynamical Jahn-Teller distortions above T_N might be quite different from the static one in the AFM phase. The last prediction can be possibly verified in future experimental studies.

V. CONCLUSIONS

In conclusion, our calculations point out at the anisotropy of quadrupole superexchange as a likely origin of noncollinear 3**k** antiferromagnetic order in UO_2 and the first-order type of the corresponding Néel transition. The present *ab initio* approach seems to be highly promising for studies of other localized f-electron systems featuring complex unexplained magnetic or "hidden" orders and local multipole degrees of freedom.

ACKNOWLEDGMENT

L.P. acknowledges the support of the European Research Council Grant No. ERC-319286-QMAC and computational resources provided by the Swedish National Infrastructure for Computing (SNIC). S.K. is grateful to Ecole Polytechnique and the Austrian CMS for financial support and to CPHT for its hospitality.

APPENDIX A: SUPEREXCHANGE IN SPHERICAL-TENSOR AND ANGULAR-MOMENT-OPERATOR FORMALISMS

In the present work we represent the dipole and quadrupole DOF of the Γ_5 triplet by the real-valued spherical tensors [4,61] $\hat{O}$ similarly to Refs. [26,27]. Some authors [7,20,50] employ instead the conventional angular-moment and quadrupole operators. The SEIs defined in the two formalisms are related to each other by simple prefactors. Namely, for the effective angular momentum $\tilde{J} = 1$ the dipole spherical tensors $\hat{O}^M = \hat{S}_M/\sqrt{2}$, where $\hat{S}_M$ is the angular-moment operator for the same projection $M = x$, y, or z, see Ref. [61]. Hence, one sees that the dipole-dipole SEIs in the angular-momentum formalism $J_{MM'}$ are related to our spherical-tensor ones by the prefactor 1/2, $J_{MM'} \equiv V_{MM'}/2$.

The quadrupole spherical tensors for $\tilde{J} = 1$ can be expressed as products of dipole ones:

$$\begin{aligned}
\hat{O}^{xy} &= -\sqrt{2}(\hat{O}^x\hat{O}^y + \hat{O}^y\hat{O}^x),\\
\hat{O}^{xz} &= \sqrt{2}(\hat{O}^x\hat{O}^z + \hat{O}^z\hat{O}^x),\\
\hat{O}^{yz} &= \sqrt{2}(\hat{O}^y\hat{O}^z + \hat{O}^z\hat{O}^x),\\
\hat{O}^{z^2} &= \sqrt{2/3}[3(\hat{O}^z)^2 - 1],\\
\hat{O}^{x^2-y^2} &= \sqrt{2}(\hat{O}^x\hat{O}^x - \hat{O}^y\hat{O}^y).
\end{aligned} \tag{A1}$$

They are converted to the corresponding quadrupole operators employed by Refs. [7,20,50] by multiplying them by $\sqrt{6}$ for z^2 and $\sqrt{2}$ for all other projections. Hence, the corresponding conversion factors between the spherical-tensors QQ SEIs V^q_M (Tables I and III) and QQ interactions K_M in Refs. [7,20,50] are 1/6 for the SEI coupling $M = z^2$, $K_{z^2} \equiv V_{z^2}/6$, and 1/2 for all other V^q_M.

The ordered states analyzed in this paper are specified by the following expectation values of the dipole tensors:

1**k** structure:

$$\langle\hat{O}^{\mathbf{R}}_x\rangle = \frac{e^{i2\pi R_y}}{\sqrt{2}}; \langle\hat{O}^{\mathbf{R}}_y\rangle = 0; \langle\hat{O}^{\mathbf{R}}_z\rangle = 0, \tag{A2}$$

2**k** structure:

$$\langle\hat{O}^{\mathbf{R}}_x\rangle = \frac{e^{i2\pi R_z}}{2}; \langle\hat{O}^{\mathbf{R}}_y\rangle = 0; \langle\hat{O}^{\mathbf{R}}_z\rangle = \frac{e^{i2\pi R_y}}{2}, \tag{A3}$$

3**k** structure:

$$\langle\hat{O}^{\mathbf{R}}_x\rangle = \frac{e^{i2\pi R_z}}{\sqrt{6}}; \langle\hat{O}^{\mathbf{R}}_y\rangle = \frac{e^{i2\pi R_x}}{\sqrt{6}}; \langle\hat{O}^{\mathbf{R}}_z\rangle = \frac{e^{i2\pi R_y}}{\sqrt{6}}, \tag{A4}$$

where **R** is the lattice vector in units of the lattice parameter a.

APPENDIX B: NEXT-NEAREST-NEIGHBORS SUPEREXCHANGE INTERACTIONS IN UO_2

The calculated SE Hamiltonian for the next-nearest-neighbor bond [001] $H^{\mathrm{NNN}}_{\mathrm{SE}} = H^{\mathrm{NNN}}_{\mathrm{DD}} + H^{\mathrm{NNN}}_{\mathrm{QQ}}$ reads

$$H^{\mathrm{NNN}}_{\mathrm{DD}} = V\sum_{M=x,y}\hat{O}^M_{\mathbf{R}}\hat{O}^M_{\mathbf{R}'} + V'\hat{O}^z_{\mathbf{R}}\hat{O}^z_{\mathbf{R}'}, \tag{B1}$$

$$H^{\mathrm{NNN}}_{\mathrm{QQ}} = \sum_{M\in t_{2g},e_g} V^q_M\hat{O}^M_{\mathbf{R}}\hat{O}^M_{\mathbf{R}'}, \tag{B2}$$

where the dipole-dipole (DD) and QQ contributions take a simpler form compared to the nearest-neighbor SE Hamiltonian [Eqs. (2) and (3) of the main text] due to the absence of off-diagonal terms. The SE Hamiltonians for other NNN bonds are obtained from that for [001] by the corresponding rotations, that amounts in the case of $H^{\mathrm{NNN}}_{\mathrm{DD}}$ to permutations of the x, y, and z labels. The $L = 2$ tensors in $H^{\mathrm{NNN}}_{\mathrm{QQ}}$ transform upon these rotations like the corresponding $l = 2$ real spherical harmonics.

The calculated values of the NNN SEIs are listed in Table III. By comparing it with Table I of the main text one sees that the NNN SEIs are about one order of magnitude smaller compared to the NN ones.

TABLE III. Calculated U-U next-nearest-neighbor interactions for the [0,0,1] bond (meV) for $J_H = 0.6$ eV.

V	V'	V^q_{xy}	$V^q_{xz(yz)}$	$V^q_{x^2-y^2}$	$V^q_{z^2}$
0.143	0.156	0.004	−0.015	−0.003	0.053

[1] N. A. Spaldin, Nat. Rev. Mater. **2**, 17017 (2017).
[2] K. I. Kugel' and D. I. Khomskii, Sov. Phys. Usp. **25**, 231 (1982).
[3] Y. Tokura, Rep. Prog. Phys. **69**, 797 (2006).
[4] P. Santini, S. Carretta, G. Amoretti, R. Caciuffo, N. Magnani, and G. H. Lander, Rev. Mod. Phys. **81**, 807 (2009).
[5] H. Kotegawa, M. Yogi, Y. Imamura, Y. Kawasaki, G.-q. Zheng, Y. Kitaoka, S. Ohsaki, H. Sugawara, Y. Aoki, and H. Sato, Phys. Rev. Lett. **90**, 027001 (2003).
[6] A. Yatskar, W. P. Beyermann, R. Movshovich, and P. C. Canfield, Phys. Rev. Lett. **77**, 3637 (1996).
[7] R. Caciuffo, P. Santini, S. Carretta, G. Amoretti, A. Hiess, N. Magnani, L.-P. Regnault, and G. H. Lander, Phys. Rev. B **84**, 104409 (2011).
[8] L. B. Skinner, C. J. Benmore, J. K. R. Weber, M. A. Williamson, A. Tamalonis, A. Hebden, T. Wiencek, O. L. G. Alderman, M. Guthrie, L. Leibowitz *et al.*, Science **346**, 984 (2014).
[9] G. J. Hutchings, C. S. Heneghan, I. D. Hudson, and S. H. Taylor, Nature (London) **384**, 341 (1996).
[10] G. Amoretti, A. Blaise, R. Caciuffo, J. M. Fournier, M. T. Hutchings, R. Osborn, and A. D. Taylor, Phys. Rev. B **40**, 1856 (1989).
[11] S. B. Wilkins, R. Caciuffo, C. Detlefs, J. Rebizant, E. Colineau, F. Wastin, and G. H. Lander, Phys. Rev. B **73**, 060406(R) (2006).
[12] R. Caciuffo, G. Amoretti, P. Santini, G. H. Lander, J. Kulda, and P. de V. Du Plessis, Phys. Rev. B **59**, 13892 (1999).
[13] E. Blackburn, R. Caciuffo, N. Magnani, P. Santini, P. J. Brown, M. Enderle, and G. H. Lander, Phys. Rev. B **72**, 184411 (2005).
[14] P. Monachesi and F. Weling, Phys. Rev. B **28**, 270 (1983).
[15] P. Burlet, J. Rossat-Mignod, S. Quezel, O. Vogt, J. Spirlet, and J. Rebizant, J. Less-Common Met. **121**, 121 (1986).
[16] K. Ikushima, S. Tsutsui, Y. Haga, H. Yasuoka, R. E. Walstedt, N. M. Masaki, A. Nakamura, S. Nasu, and Y. Ōnuki, Phys. Rev. B **63**, 104404 (2001).
[17] H. Nakotte, R. Rajaram, S. Kern, R. J. McQueeney, G. H. Lander, and R. A. Robinson, J. Phys.: Conf. Ser. **251**, 012002 (2010).
[18] P. Giannozzi and P. Erdös, J. Magn. Magn. Mater. **67**, 75 (1987).
[19] G. Solt and P. Erdös, Phys. Rev. B **22**, 4718 (1980).
[20] V. Mironov, L. Chibotaru, and A. Ceulemans, *Advances in Quantum Chemistry* (Academic, New York, 2003), Vol. 44, pp. 599–616.
[21] M.-T. Suzuki, H. Ikeda, and P. M. Oppeneer, J. Phys. Soc. Jpn. **87**, 041008 (2018).
[22] N. Magnani, M.-T. Suzuki, and P. M. Oppeneer, C. R. Phys. **15**, 580 (2014).
[23] M.-T. Suzuki, N. Magnani, and P. M. Oppeneer, Phys. Rev. B **88**, 195146 (2013).
[24] F. Bultmark, F. Cricchio, O. Grånäs, and L. Nordström, Phys. Rev. B **80**, 035121 (2009).
[25] F. Zhou and V. Ozoliņš, Phys. Rev. B **80**, 125127 (2009).
[26] S.-T. Pi, R. Nanguneri, and S. Savrasov, Phys. Rev. Lett. **112**, 077203 (2014).
[27] S.-T. Pi, R. Nanguneri, and S. Savrasov, Phys. Rev. B **90**, 045148 (2014).
[28] A. Georges, G. Kotliar, W. Krauth, and M. J. Rozenberg, Rev. Mod. Phys. **68**, 13 (1996).
[29] V. I. Anisimov, F. Aryasetiawan, and A. I. Lichtenstein, J. Phys.: Condens. Matter **9**, 767 (1997).
[30] A. I. Lichtenstein and M. I. Katsnelson, Phys. Rev. B **57**, 6884 (1998).
[31] G. Kotliar, S. Y. Savrasov, K. Haule, V. S. Oudovenko, O. Parcollet, and C. A. Marianetti, Rev. Mod. Phys. **78**, 865 (2006).
[32] J. Kolorenč, A. B. Shick, and A. I. Lichtenstein, Phys. Rev. B **92**, 085125 (2015).
[33] N. Lanatà, Y. Yao, X. Deng, V. Dobrosavljević, and G. Kotliar, Phys. Rev. Lett. **118**, 126401 (2017).
[34] L. V. Pourovskii, Phys. Rev. B **94**, 115117 (2016).
[35] M. Aichhorn, L. Pourovskii, V. Vildosola, M. Ferrero, O. Parcollet, T. Miyake, A. Georges, and S. Biermann, Phys. Rev. B **80**, 085101 (2009).
[36] M. Aichhorn, L. Pourovskii, and A. Georges, Phys. Rev. B **84**, 054529 (2011).
[37] P. Blaha, K. Schwarz, G. Madsen, D. Kvasnicka, and J. Luitz, *WIEN2k, An augmented Plane Wave + Local Orbitals Program for Calculating Crystal Properties* (Techn. Universitat Wien, Austria, 2001).
[38] O. Parcollet, M. Ferrero, T. Ayral, H. Hafermann, I. Krivenko, L. Messio, and P. Seth, Comput. Phys. Commun. **196**, 398 (2015).
[39] M. Aichhorn, L. Pourovskii, P. Seth, V. Vildosola, M. Zingl, O. E. Peil, X. Deng, J. Mravlje, G. J. Kraberger, C. Martins *et al.*, Comput. Phys. Commun. **204**, 200 (2016).
[40] K. T. Moore and G. van der Laan, Rev. Mod. Phys. **81**, 235 (2009).
[41] P. Seth, P. Hansmann, A. van Roekeghem, L. Vaugier, and S. Biermann, Phys. Rev. Lett. **119**, 056401 (2017).
[42] J. Hubbard, Proc. R. Soc. London Sect. A **276**, 238 (1963).
[43] L. V. Pourovskii, B. Amadon, S. Biermann, and A. Georges, Phys. Rev. B **76**, 235101 (2007).
[44] M. T. Czyżyk and G. A. Sawatzky, Phys. Rev. B **49**, 14211 (1994).
[45] P. Delange, S. Biermann, T. Miyake, and L. Pourovskii, Phys. Rev. B **96**, 155132 (2017).
[46] S.-W. Yu, J. G. Tobin, J. C. Crowhurst, S. Sharma, J. K. Dewhurst, P. Olalde-Velasco, W. L. Yang, and W. J. Siekhaus, Phys. Rev. B **83**, 165102 (2011).
[47] X. Dai, K. Haule, and G. Kotliar, Phys. Rev. B **72**, 045111 (2005).
[48] H. Ogasawara, A. Kotani, and B. T. Thole, Phys. Rev. B **44**, 2169 (1991).
[49] The observable dipole magnetic and quadrupole moments are related to the corresponding tensor moments defined in the Γ_5 basis (2) by the prefactors 2.88, 0.153, and 0.217 for the dipole, quadrupole e_g, and quadrupole t_{2g}, respectively.
[50] S. Carretta, P. Santini, R. Caciuffo, and G. Amoretti, Phys. Rev. Lett. **105**, 167201 (2010).
[51] M. Rotter, J. Magn. Magn. Mater. **272-276**, E481 (2004).
[52] Using the SEIs evaluated with $J_H = 0.7$ eV we obtain the same ordered structures at almost identical temperature of 54 K.
[53] W. Minor and T. M. Giebultowicz, J. Phys. Colloques **49**, C8-1551 (1988).

[54] H. T. Diep and H. Kawamura, Phys. Rev. B **40**, 7019 (1989).
[55] J. Jensen and P. Bak, Phys. Rev. B **23**, 6180 (1981).
[56] T. Oguchi, Prog. Theor. Phys. **13**, 148 (1955).
[57] S. Khmelevskyi, Phys. Rev. B **86**, 104429 (2012).
[58] E. L. Nagaev and A. A. Kovalenko, JETP Lett. **29**, 492 (1979).
[59] A. A. Kovalenko and E. L. Nagaev, JETP Lett. **35**, 24 (1982).
[60] E. L. Nagaev, Sov. Phys. Usp. **25**, 31 (1982).
[61] K. Blum, *Density Matrix Theory and Applications* (Plenum, New York, 1996).